Evidence for a Peierls phase-transition in a three-dimensional multiple charge-density waves solid

Barbara Mansart[a,b], Mathieu J. G. Cottet[a], Thomas J. Penfold[b,c,d], Stephen B. Dugdale[e], Riccardo Tediosi[f], Majed Chergui[b], and Fabrizio Carbone[a,1]

[a]Laboratory for Ultrafast Microscopy and Electron Scattering, Institute of Condensed-Matter Physics, Ecole Polytechnique Fédérale de Lausanne, CH-1015 Lausanne, Switzerland; [b]Laboratory of Ultrafast Spectroscopy, Institute of Chemical Sciences and Engineering, Ecole Polytechnique Fédérale de Lausanne, CH-1015 Lausanne, Switzerland; [c]Laboratory of Computational Chemistry and Biochemistry, Institute of Chemical Sciences and Engineering, Ecole Polytechnique Fédérale de Lausanne, CH-1015 Lausanne, Switzerland; [d]SwissFEL, Paul Scherrer Institute, CH-5232 Villigen, Switzerland; [e]H. H. Wills Physics Laboratory, University of Bristol, Tyndall Avenue, Bristol BS8 1TL, United Kingdom; and [f]Département de Physique de la Matière Condensée, Université de Genève, CH-1211 Geneva 4, Switzerland

The effect of dimensionality on materials properties has become strikingly evident with the recent discovery of graphene. Charge ordering phenomena can be induced in one dimension by periodic distortions of a material's crystal structure, termed Peierls ordering transition. Charge-density waves can also be induced in solids by strong coulomb repulsion between carriers, and at the extreme limit, Wigner predicted that crystallization itself can be induced in an electrons gas in free space close to the absolute zero of temperature. Similar phenomena are observed also in higher dimensions, but the microscopic description of the corresponding phase transition is often controversial, and remains an open field of research for fundamental physics. Here, we photoinduce the melting of the charge ordering in a complex three-dimensional solid and monitor the consequent charge redistribution by probing the optical response over a broad spectral range with ultrashort laser pulses. Although the photoinduced electronic temperature far exceeds the critical value, the charge-density wave is preserved until the lattice is sufficiently distorted to induce the phase transition. Combining this result with ab initio electronic structure calculations, we identified the Peierls origin of multiple charge-density waves in a three-dimensional system for the first time.

ultrafast broadband spectroscopy | electron-lattice interactions | optical spectral weight

Charge ordering phenomena occurring upon symmetry breaking are important in solids as they give rise to current and spin flow patterns in promising materials such as organic conductors (1), multilayered graphene (2) and transition metal oxides (3). The possibility to investigate the microscopic steps through which such ordering transition occurs also gives the opportunity to speculate on more general aspects of critical phenomena. Charge-density waves (CDWs) (4, 5), sandpile automata (6), and Josephson arrays (7) have been investigated in relation to the scale invariance of self-organized critical phenomena (8), of which avalanches are dramatic manifestations (9). In one dimension, Peierls demonstrated that at low temperature an instability can be induced by the coupling between carriers and a periodic lattice distortion. Such an instability triggers a charge ordering phenomenon and a metal-insulator phase transition, called Peierls transition, occurs (10). Like for Bardeen–Cooper–Schrieffer (BCS) superconductors, such an electron–phonon interaction-driven transition is expected to be second order (10). Although this situation is fairly established in monodimensional organic materials (11), increased hybridization leading to higher dimensionality of a solid perturbs this scenario and makes the assessment of the microscopic origin of charge localization phenomena more difficult (12–14).

Contrary to other low-dimensional CDW (15) systems studied so far by time-resolved spectroscopies (16–19), $Lu_5Ir_4Si_{10}$ presents a complex three-dimensional structure with several substructures such as one-dimensional Lu chains and three-dimen-

sional cages in which a variety of many-body effects (including superconductivity) originate (20) (Fig. 1A). Although a CDW occurs below $T_{CDW} = 83$ K, its microscopic origin is still debated because this transition is first order and isotropic without hysteresis (21, 22), in contrast to the standard Peierls paradigm. Also, owing to their complexity, a detailed microscopic description of the properties of these solids is still lacking and their band structure has never been reported.

The charge redistribution induced by a phase transition in a solid can be obtained via the optical frequency-sum rule (22), which states that the integral over all frequencies of the optical conductivity $[\sigma_1(\omega)]$, termed spectral weight (SW), is constant and corresponds to the number of electrons per unit cell:

$$\text{SW} = \frac{\pi e^2}{2 m_e V} N_{eff} = \int_0^\infty \sigma_1(\omega)d\omega, \qquad [1]$$

where m_e is the free electron mass, V the unit cell volume, and N_{eff} the total number of carriers. Performing the integral up to a frequency cutoff Ω_c (partial sum rule) gives the number of carriers contained in the electronic levels included in this energy range (see *SI Text*). Optical weight redistributions are known to accompany every BCS-like phase transition, as described by the Ferrel–Glover–Tinkham sum rule (23). Recently, it has been shown that information on the SW can be obtained in a model-independent fashion based on the analytical continuation of holomorphic functions (24).

In this study, we aim at obtaining the temporal evolution of the partial sum rule during the photoinduced annihilation of the CDW order parameter to identify the different states through which the electronic and the lattice structure evolve. To perform this study, the changes in the optical constants are monitored over a broad energy range with a temporal resolution better than the electron–phonon coupling time. We performed pump-probe reflectivity using a broad (1.5–3 eV) supercontinuum of 50 fs polarized pulses as a probe (*SI Text*). The temperature of the sample was controlled between 10 K and room temperature. The 1.55 eV pump fluence was varied between 0.8 and 3.1 mJ/cm², corresponding to an absorbed fluence between 0.4 and 1.55 mJ/cm²; in these conditions and for an initial temperature of 10 K, the electronic temperature reaches values between 302 and 1,100 K (see the transient temperature analysis below), corresponding to

PHYSICS

energies in the range of 26–94 meV. Therefore, for the lowest pump fluences, the absorbed energy lies below the CDW gap estimated by static optical spectroscopy (80 meV) (22). Our ultrafast reflectivity data were combined with static optical spectroscopy (22) and ab initio band structure calculations, allowing the identification of the spectroscopic signature of the CDW melting, the description of the orbitals and atomic motions involved, and their temporal evolution.

The static optical reflectivity of $Lu_5Ir_4Si_{10}$ for light polarized along the one-dimensional chains (c axis), and perpendicular to them (a axis) is displayed in Fig. 1B. Fig. 1C shows the calculated reflectivity, which agrees with the experiments; some discrepancies are observed at low energy along the c axis where correlation effects are expected due to the presence of the monodimensional chains. Fig. 1 D–G shows the transient optical reflectivity for different temperatures and light polarizations. The low-temperature dynamic reflectivity decays faster than at room temperature (200 fs compared with 300 fs, for the same pump fluence and energy of 1.9 eV). Its spectral behavior is also rather different: At 10 K, a large region is observed in which the photoinduced change in reflectivity switches sign (see white traces). The time-scales and the absolute magnitude of the changes also depend on the polarization of the probe.

The evolution of N_{eff} is obtained from the transient reflectivity both via a Drude–Lorentz model (3D color maps in Fig. 2) and the model-independent approach (white lines with error bars in Fig. 2 A and B) (SI Text). In these plots, the integral in Eq. 1 is displayed as a function of the frequency cutoff, emphasizing the spectral regions of positive and negative change of the effective number of carriers. When the sample temperature is below T_{CDW} and the probe light is polarized along the c axis (Fig. 2B), the N_{eff} change, defined as $(N_{eff}(t, \omega) - N_{eff}(t < 0, \omega))$, becomes negative after 200 fs. Instead, it is always positive when the polarization is perpendicular to the c axis (Fig. 2A) or at room temperature (Fig. 2C). This sign change at low temperature along the c axis signals an SW transfer from energies higher than 1.5 eV, typical of strongly correlated solids (25). In Fig. 2 D and E, the quantities $(N_{eff}(T_2, \omega) - N_{eff}(T_1, \omega))/N_{eff}(T_1, \omega)$ are displayed for $T_1 = 60$ K and $T_2 = 120$ K, with light polarized along the c axis (red line) or the a axis (black line), and $T_1 = 120$ K and $T_2 = 290$ K for light polarized along the c axis (light-blue line) (data taken from ref. 22). The SW transfer across the CDW temperature along the c axis becomes negative above 1.5 eV, as

observed in the transient data; therefore, the spectroscopic signature of the CDW melting is the redistribution of carriers above 1.5 eV where bands composed of Lu and Ir 5d states are found. Remarkably, we observe that this feature appears several tens of femtoseconds after laser excitation, suggesting that, before the CDW melts, an unconventional state of matter is produced in which some charge order survives despite the large energy deposited in the electronic subsystem.

To verify that indeed the behavior of the optical constants in the 2- to 3-eV region is mainly sensitive to the CDW melting, we measured the transient reflectivity spectra at different fluences (0.8–3.1 mJ/cm^2) and temperatures (10, 80, and 300 K). In Fig. 3 B and C, the transient reflectivity at 1.77 and 2.21 eV are shown for the different pump fluences. At 1.77 eV, the reflectivity changes are always positive, whereas at 2.21 eV a negative dip develops at fluences higher than 2.1 mJ/cm^2. In Fig. 3D, the temperature dependence of the transient reflectivity is also shown, at a probe energy of 2.21 eV and for a fluence of 3.1 mJ/cm^2. Also in this case, the change of reflectivity has a negative part, associated to the CDW melting, at 10 K, whereas it is always positive at temperatures higher than T_{CDW}.

The time scales involved in the melting of the CDW are obtained through a transient temperature analysis using the three-temperature model (26, 27), appropriate for anisotropic materials with selective electron–phonon coupling (28–30). This model describes the energy transfer from excited carriers to the lattice as an effective heat exchange between them. We obtained the temporal evolution of electronic and lattice temperatures (SI Text) and display them in Fig. 3A together with the transient ΔN_{eff} at 10 K and polarization along the c axis. The CDW melting, indicated by ΔN_{eff} becoming negative at high energy, occurs after the lattice reaches a temperature above T_{CDW}. While the electronic temperature T_e crosses T_{CDW} and reaches values as high as 1,100 K, the system exists in a transient state where the signature of the molten CDW state is still absent. These simulations provide an estimate of the Eliashberg electron–phonon coupling parameter $\lambda \approx 0.6$ and a fraction of strongly coupled modes (approximately 20%), in agreement with the value of $\lambda = 0.66$ determined by combined heat capacity and magnetic susceptibility measurements under pressure (31). The rise time of our $\Delta R/R$ signal is in our temporal resolution range—i.e., 40–50 fs. This observation, together with the three-temperature model simulations, provides an estimate of the excited electron thermalization
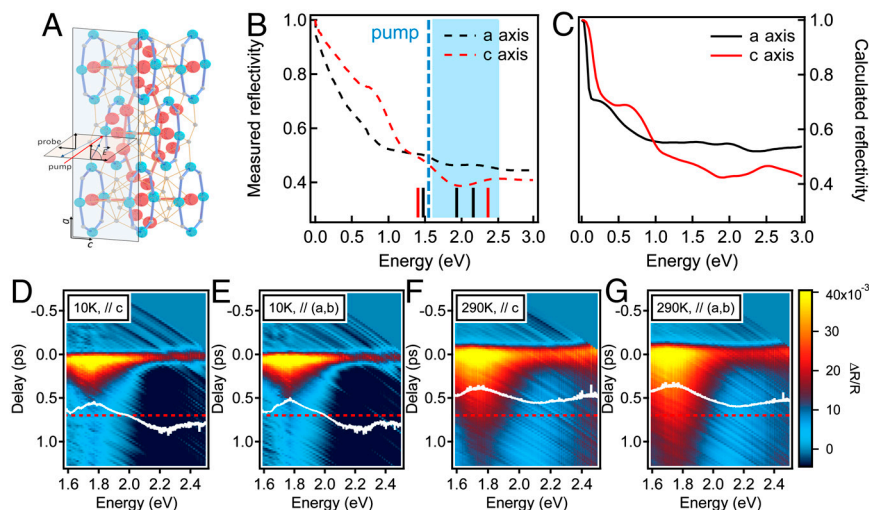

Fig. 1. (A) Experimental geometry and crystal structure; the pump and probe polarizations can be varied independently. (B) Static reflectivity measurements; vertical bars indicate the optical absorptions of the solid, the vertical dashed line the energy of our photoexciting pulse, and the probe supercontinuum range is highlighted as a light-blue shaded area, covering a spectral region of large anisotropy. (C) Calculated reflectivity along the a and the c axes. (D–G) Time-resolved reflectivity images for a pump fluence of 3.1 mJ/cm^2 and (D and E) $T = 10$ K, (F and G) $T = 290$ K. White traces in D–G are profiles extracted at 700 fs, whose baselines are shown as dashed red lines.
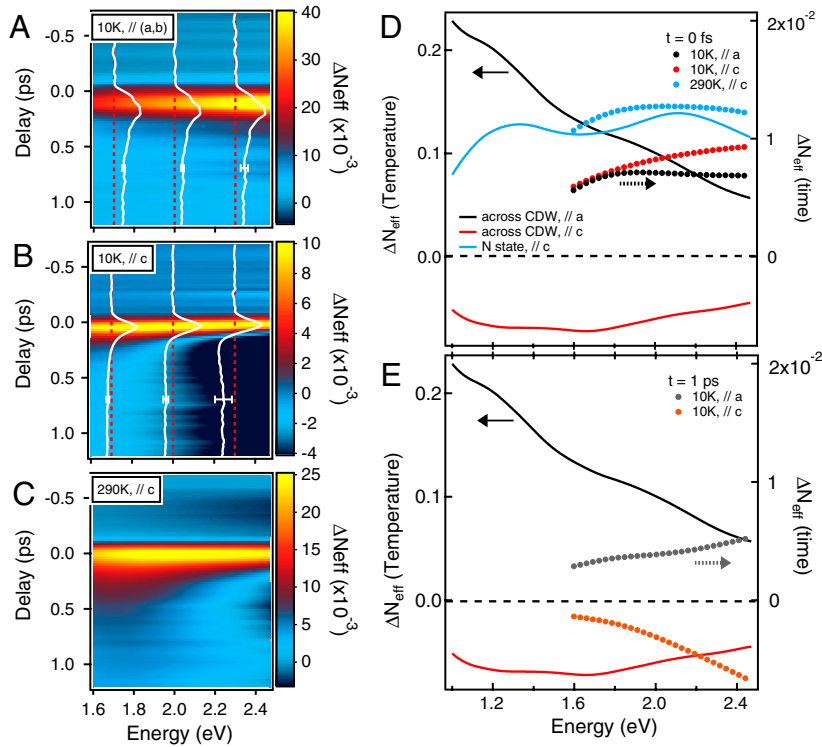
Fig. 2. Spectral weight analysis. (*A–C*) Three-dimensional color maps of time-resolved N_{eff}. (*D* and *E*) Difference in N_{eff} between the normal (*T* = 120 K) and the charge-density wave (*T* = 60 K) states for the two orientations, and between two different temperatures in the normal state (290–120 K) (solid lines); time-resolved N_{eff} for *T* = 10 and 290 K, and probe parallel to *c* or *a* axis (circles), at time delays of 0 fs (*D*) and 1 ps (*E*).

time around 50 fs, much faster than the CDW melting time. This difference in timescales rules out any possible electronic melting because, in this case, a clear signature of the molten CDW state should be present as early as the electron thermalization time, as recently observed in TaS_2 (32).

To speculate on the microscopic nature of the intermediate state, we consider that during the first 200 fs the electronic struc-

ture is relaxing after being put abruptly out-of-equilibrium by the pump pulse. By comparing the spectra of the photoinduced reflectivity changes at different time delays to the difference spectra between the static reflectivity recorded at different temperatures, the impact of the out-of-equilibrium electronic structure can be estimated. In Fig. 4*A*, the transient reflectivity spectra at 60, 120, 200, and 500 fs after excitation are displayed together with R
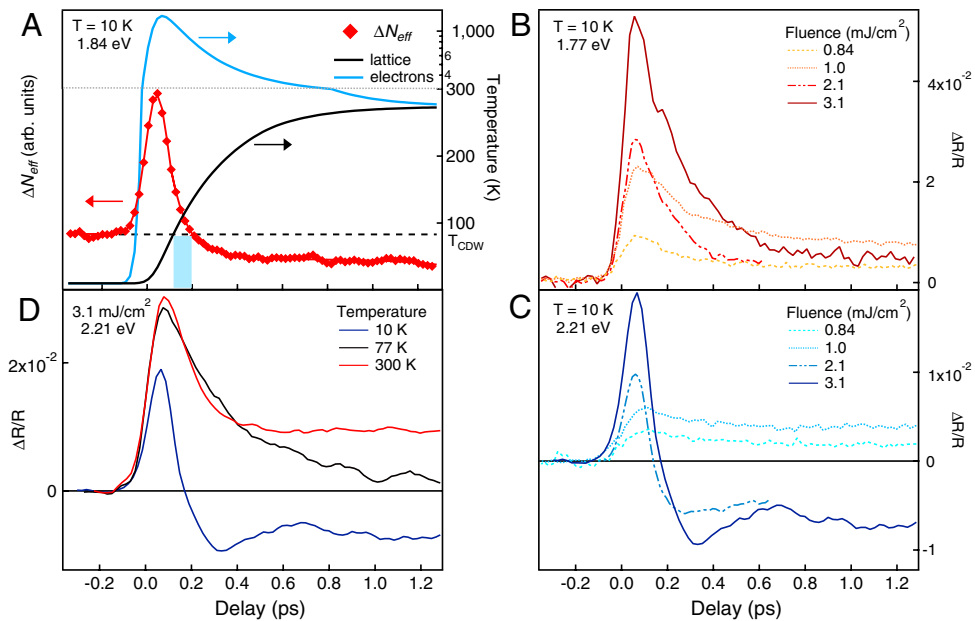

Fig. 3. (*A*) Time-dependent lattice (black) and electronic (blue) temperatures, obtained by solving the three-temperature model for *T* = 10 K, *F* = 3.1 mJ/cm^2, an energy of 1.84 eV, and corresponding transient N_{eff}. The dashed line represents the zero baseline for N_{eff} and the CDW transition temperature. (*B* and *C*) Fluence dependence of the transient reflectivity traces at 10 K and 1.77 eV (*B*) and 2.21 eV (*C*) probing wavelengths. (*D*) Temperature dependence of the transient reflectivity at 3.1 mJ/cm^2 pumping fluence and 2.21 eV probing wavelength.
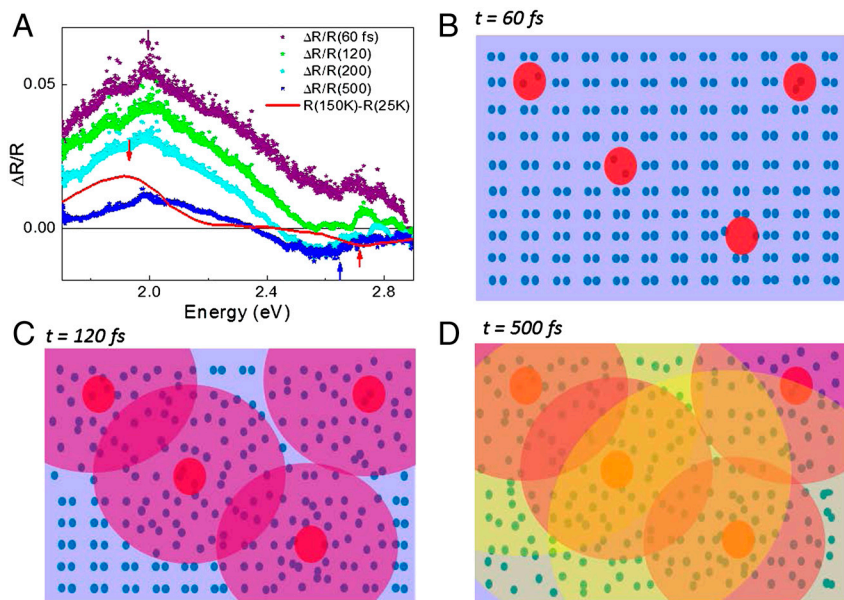
Fig. 4. Transient state. (*A*) Transient reflectivity spectra at 60, 120, 200, and 500 fs respectively, colored asterisks. Static temperature difference spectra, R (150 K)–R(25 K), continuous line. (*B–D*) Cartoon of the CDW melting dynamics. The colored areas indicate the regions where excitation perturbs the charge order.

(150 K)–R(25 K). When the electronic structure and the lattice are at equilibrium, the temperature difference spectrum exhibits a positive peak around 2 eV and a minimum around 2.7 eV across the phase transition (red line). This behavior is quite similar to that of the transient reflectivity after 500 fs, at which time the electronic structure is likely at equilibrium with the lattice. $\Delta R/R$ also shows a positive peak around 2 eV and a negative minimum around 2.7 eV; this similarity indicates that photoexcitation and temperature induce the same carriers redistribution in the solid. At early times, when the shape of the transient spectra is still similar to the static one showing a positive peak around 2 eV and a minimum around 2.7 eV, a quantitative discrepancy is more pronounced and could originate from the very large electronic temperature jump induced by laser excitation (>1,000 K) compared to the static case in which the system is heated by 100°. These spectra suggest that, consistently with the three-temperature model analysis, a thermal electronic distribution of carriers is established within few tens of femtoseconds.

It is important to note at this point that although a negative reflectivity change can be associated to the phase transition, the complete melting of the CDW state can only be claimed when the optical SW, which is the cumulative effect of the positive and negative changes, becomes negative. At a fluence of 3.1 mJ/cm^2, around one carrier per unit cell is photoexcited. Photoexcited carriers create "hot areas" in which the CDW can be perturbed. This electronic perturbation diffuses in space via its interaction with the lattice and after some time, a thermally CDW molten state is reached. The delay of this process is governed by the microscopic details of the coupling between carriers and phonons in the CDW state. This scenario is pictorially represented in the cartoon in Fig. 4 *B–D*.

The presented situation is very distinct from an electronically driven melting of the charge order, because in that case the negative optical SW should be observable without any delay; therefore, even though an instantaneous (<60 fs) CDW melting would locally happen upon light excitation, it should propagate and melt the whole charge order within the electronic thermalization time, which we found to be around 60 fs. Such a situation is observed for example in TaS$_2$ (32), where a non-Peierls phase transition is claimed to take place.

Further microscopic details are obtained through ab initio electronic structure calculations (*SI Text*), performed via both an all-electron full-potential linearized augmented plane-wave method (http://elk.sourceforge.net/) and via pseudopotentials (33). Eleven bands having mixed character (color coded in Fig. 5*B*) cross the Fermi level. The density of states (DOS) (Fig. 5*B*) shows that the Fermi surface has mostly Ir 5*d* character. Some Lu character is found, coming from the 5*d* orbitals strongly hybridized with both Si and Ir, producing delocalized electrons as observed in transition metal-silicides (34). The Fermi surface is presented in Fig. 5*A*, and from calculations of the generalized susceptibility, we identified two bands having nesting vectors of 2/7 and 3/7 of c^*, as observed by X-ray diffraction below T_{CDW} (21). These two nested bands suggest the presence of multiple CDWs occurring at the same transition temperature. These two nested bands account for approximately 30% of the Fermi energy DOS, in agreement with estimates based on magnetic susceptibility measurements (31). Whereas one of them comes mostly from Ir $5d_{z^2}$ and Lu1 $5d_{yz}$ (Lu1 atoms being along the chains, ref. 21; Fig. 5*C*), the second one is mainly formed by Lu2 $5d_{yz}$–$5d_{z^2}$ and all the 5*d* orbitals of both Lu3 and Ir. This complex and three-dimensional nature of the orbitals reveals the possibility of a 3D Peierls transition. We also show in Fig. 5*C* the motion of two strongly coupled optical phonons, yellow and orange arrows respectively, having frequencies (1.4 and 2.8 THz) close to the coherent oscillations observed in the same material.* Ab initio calculations also estimate the electron–phonon coupling parameter of each individual lattice mode, yielding a total $\lambda \approx 0.6$ for the 18% of the most coupled modes, in agreement with the three-temperature model simulations.

The orbital occupation-number change induced by the CDW melting is signaled by the optical SW transfer around a pivot energy close to 1 eV, both in static and time-resolved data. Upon excitation, acting as a photodoping process, carriers are transferred from the Lu and Ir 5*d* states forming the CDW (*SI Text*). This transfer depopulates the nested bands and redistributes the excited carriers above the Fermi level, increasing the

*Tomeljak A, et al., Femtosecond Real-Time Studies of Lu$_5$Ir$_4$Si$_{10}$ Charge Density Wave Compound, Workshop on Recent Developments in Low Dimensional Charge Density Wave Conductors, June 29–July 3, 2006, Skradin, Croatia.
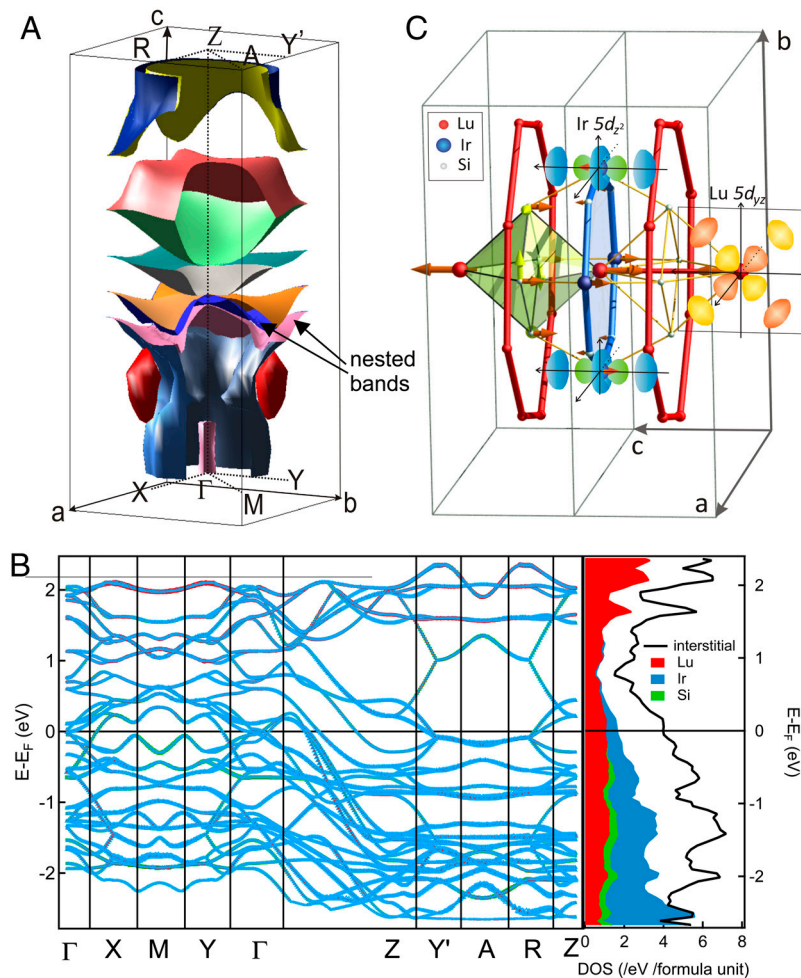
Mansart et al.

Fig. 5. Electronic structure calculations. (*A*) Three-dimensional map of the Fermi surface. (*B*) Band structure with atomic character and partial density of states. (*C*) Representation of the main atomic orbitals (Ir $5d_{z^2}$ and Lu $5d_{yz}$) forming one of the nested bands, and atomic movement of two of the most coupled phonon modes (thick orange and yellow arrows). Lu1 atoms form chains along the *c* axis, Lu2 the ring in the (*a, b*) plane, and Lu3 (not represented) are more three-dimensionally distributed.

low-energy SW as well as the effective electronic temperature. The observation of a delay between photoexcitation and the melting of the CDW strongly suggests the Peierls nature of the phase transition in these compounds, rather than a pure electronic effect as in different systems (35). In fact, whereas CDW are known to couple to specific lattice distortions, the intimate microscopic origin of the mechanism described in ref. 10 is that a periodic modulation of the lattice induces the Fermi surface instability causing the consequent charge ordering. In other words, to understand correctly the origin of such a phase transition, a notion of causality must be invoked, which is directly obtainable via time-resolved experiments. Indeed, one must wait until the atoms have moved sufficiently to suppress the distortion promoting the CDW state (18, 36); the latency time can be of the order of one-quarter of the corresponding phonon period. In our case, 200 fs gives a frequency of 1.4 THz, corresponding to the mode represented in orange arrows in Fig. 5*C*. Although the direct involvement of the lattice in the CDW formation reveals the Peierls nature of the metal-insulator transition in this material, its weakly one-dimensional electronic structure, together with the signatures of a first-order CDW transition and the suggested presence of multiple CDWs, are at odds with the conventional scenario describing Peierls transitions (15). Recently, the notion that Peierls transitions can happen in higher dimensions has been challenged by ultrafast experiments in TaS$_2$ (32), which has a 2D charge ordering transition. Also in this case, the delay between

excitation and melting has been used as the key argument for determining the microscopic nature of the phase transition. Our experiments contribute to this exciting and current debate by showing evidence for a Peierls transition in a three-dimensional system.

The proper description of phase transitions is important for fundamental physics; in fact, phase transitions in complex systems often evolve through several unconventional intermediate states (37). Critical phenomena involving abrupt perturbation of ordered systems are observed in giant landslides (9) and sandpile automata (6). In these cases and in CDWs, an external perturbation may induce a transient state in which the order is preserved while undergoing a collective reorganization (4, 5). The speed of rock slides, CDW slides, and flux jumps in the vortex state of type II superconductors are self-organized critical phenomena and obey similar critical laws (4, 7, 8, 38). In our experiments, the disappearance of the charge order manifests itself after a significant delay from the abrupt perturbation, and in the intermediate state, the order seems preserved despite the large energy deposited.

PHYSICS

1. Lorenz T, et al. (2002) Evidence for spin-charge separation in quasi-one-dimensional organic conductors. *Nature* 418:614–617.
2. Ho CH, et al. (2010) Magneto-electronic properties of rhombohedral trilayer graphene: Peierls tight-binding model. *Ann Phys* 326:721–739.
3. Qazilbash MM, et al. (2011) Nanoscale imaging of the electronic and structural transitions in vanadium dioxide. *Phys Rev B Condens Matter Mater Phys* 83:165108.
4. Middleton AA, Biham O, Littlewood PB, Sibani P (1992) Complete mode locking in models of charge-density waves. *Phys Rev Lett* 68:1586–1589.
5. Narayan O, Middleton AA (1994) Avalanches and the renormalization group for pinned charge-density waves. *Phys Rev B Condens Matter Mater Phys* 49:244–256.
6. Tadić B, Nowak U, Usadel KD, Ramaswamy R, Padlewski S (1992) Scaling behavior in disordered sandpile automata. *Phys Rev A* 45:8536–8545.
7. Benz SP, Rzchowski MS, Tinkham M, Lobb CJ (1990) Fractional giant Shapiro steps and spatially correlated phase motion in 2D Josephson arrays. *Phys Rev Lett* 64:693–696.
8. Bak P, Tang C, Wiesenfeld K (1987) Self-organized criticality: An explanation of the $1/f$ noise. *Phys Rev Lett* 59:381–384.
9. Kilburn CRJ, Petley DN (2003) Forecasting giant, catastrophic slope collapse: Lessons from Vajont, Northern Italy. *Geomorphology* 54:21–32.
10. Peierls RE (1955) *Quantum Theory of Solids* (Oxford Univ Press, London).
11. Coleman LB (1973) Superconducting fluctuations and the peierls instability in an organic solid. *Solid State Commun* 12:1125–1132.
12. Ong NP, Monceau P (1977) Anomalous transport properties of a linear-chain metal: $NbSe_3$. *Phys Rev B Condens Matter Mater Phys* 16:3443–3455.
13. Moncton DE, Axe JD, DiSalvo FJ (1975) Study of superlattice formation in $2H$-$NbSe_2$ and $2H$-$TaSe_2$ by neutron scattering. *Phys Rev Lett* 34:734–737.
14. McMillan WL (1977) Microscopic model of charge-density waves in $2H$-$TaSe_2$. *Phys Rev B Condens Matter Mater Phys* 16:643–650.
15. Grüner G (1988) The dynamics of charge-density waves. *Rev Mod Phys* 60:1129–1181.
16. Yusupov R, et al. (2010) Coherent dynamics of macroscopic electronic order through a symmetry breaking transition. *Nat Phys* 6:681–684.
17. Eichberger M, et al. (2010) Snapshots of cooperative atomic motions in the optical suppression of charge density waves. *Nature* 468:799–802.
18. Schmitt F, et al. (2008) Transient electronic structure and melting of a charge density wave in $TbTe_3$. *Science* 321:1649–1652.
19. Tomeljak A, et al. (2009) Dynamics of photoinduced charge-density-wave to metal phase transition in $K_{0.3}MoO_3$. *Phys Rev Lett* 102:066404.
20. van Smaalen S, et al. (2004) Multiple charge-density waves in $R_5Ir_4Si_{10}$ (R = Ho, Er, Tm, and Lu). *Phys Rev B Condens Matter Mater Phys* 69:014103.
21. Becker B, et al. (1999) Strongly coupled charge-density wave transition in single-crystal $Lu_5Ir_4Si_{10}$. *Phys Rev B Condens Matter Mater Phys* 59:7266–7269.
22. Tediosi R, et al. (2009) Evidence for strongly coupled charge-density-wave ordering in three-dimensional $R_5Ir_4Si_{10}$ compounds from optical measurements. *Phys Rev B Condens Matter Mater Phys* 80:035107.
23. Tinkham M, Ferrell RA (1959) Determination of the superconducting skin depth from the energy gap and sum rule. *Phys Rev Lett* 2:331–333.
24. Kuzmenko AB, van der Marel D, Carbone F, Marsiglio F (2007) Model-independent sum rule analysis based on limited-range spectral data. *New J Phys* 9:229.
25. Rozenberg MJ, Kotliar G, Kajueter H (1996) Transfer of spectral weight in spectroscopies of correlated electron systems. *Phys Rev B Condens Matter Mater Phys* 54:8452–8468.
26. Kaganov MI, Lifshitz IM, Tanatarov LV (1957) Relaxation between electrons and the crystalline lattice. *Sov Phys JETP* 4:173–178.
27. Allen PB (1987) Theory of thermal relaxation of electrons in metals. *Phys Rev Lett* 59:1460–1463.
28. Perfetti L, et al. (2007) Ultrafast electron relaxation in superconducting $Bi_2Sr_2CaCu_2O_{8+\delta}$ by time-resolved photoelectron spectroscopy. *Phys Rev Lett* 99:197001.
29. Mansart B, et al. (2010) Ultrafast transient response and electron-phonon coupling in the iron-pnictide superconductor $Ba(Fe_{1-x}Co_x)_2As_2$. *Phys Rev B Condens Matter Mater Phys* 82:024513.
30. Carbone F, Yang DS, Giannini E, Zewail AH (2008) Direct role of structural dynamics in electron-lattice coupling of superconducting cuprates. *Proc Natl Acad Sci USA* 105:20161–20166.
31. Shelton RN, et al. (1986) Electronic phase transition and partially gapped Fermi surface in superconducting $Lu_5Ir_4Si_{10}$. *Phys Rev B Condens Matter Mater Phys* 34:4590–4594.
32. Petersen JC, et al. (2011) Clocking the melting transition of charge and lattice order in $1T$-TaS_2 with ultrafast extreme-ultraviolet angle-resolved photoemission spectroscopy. *Phys Rev Lett* 107:177402.
33. Giannozzi P, et al. (2009) QUANTUM ESPRESSO: A modular and open-source software project for quantum simulations of materials. *J Phys Condens Matter* 21:395502.
34. Carbone F, et al. (2006) Electronic structure of MnSi: The role of electron-electron interactions. *Phys Rev B Condens Matter Mater Phys* 73:085114.
35. Wentzcovitch RM, Schulz WW, Allen PB (1994) VO_2: Peierls or Mott-Hubbard? A view from band theory. *Phys Rev Lett* 72:3389–3392.
36. Cavalleri A, Dekorsy Th, Chong HHW, Kieffer JC, Schoenlein RW (2004) Evidence for a structurally-driven insulator-to-metal transition in VO_2: A view from the ultrafast timescale. *Phys Rev B Condens Matter Mater Phys* 70:161102(R).
37. Baum P, Yang D-S, Zewail AH (2007) 4D visualization of transitional structures in phase transformations by electron diffraction. *Science* 318:788–792.
38. Richard J, Monceau P, Renard M (1982) Charge-density-wave motion in $NbSe_3$. II. Dynamical properties. *Phys Rev B Condens Matter Mater Phys* 25:948–970.